Journal of Advanced Ceramics
2014, 3(2): 155–164
DOI: 10.1007/s40145-014-0107-z

ISSN 2226-4108
CN 10-1154/TQ

Research Article

Influence of Fe_2O_3 on the physical, structural and electrical properties of sodium lead borate glasses

Safeya IBRAHIM[a], Mohamed Mahmoud GOMAA[b,*], Hussein DARWISH[a]

[a]*Glass Research Department*, *National Research Centre*, *Dokki*, *Cairo*, *Egypt*
[b]*Geophysical Sciences Department*, *National Research Centre*, *Dokki*, *Cairo*, *Egypt*

Received: March 19, 2014; Revised: April 24, 2014; Accepted: April 27, 2014

Abstract: The influence of adding Fe_2O_3 at the expense of Na_2O in sodium lead borate glasses on the structural, physical and electrical properties have been investigated. Results obtained from Fourier transform infrared (FTIR) spectra indicated that Fe_2O_3 plays an important role in converting three coordinated boron atoms [BO_3] to four coordinated boron atoms [BO_4]. The physical properties such as density and molar volume helped to evaluate the compact structure of the prepared glass samples due to presence of [BO_4] groups. The increase of Fe_2O_3/Na_2O replacements led to increasing the microhardness values and decreasing the thermal expansion coefficients of the studied glasses. The increase of Fe_2O_3/Na_2O replacements generally decreased the AC conductivity. That decrease might be due to converting of the three coordinated boron atoms [BO_3] to four coordinated boron atoms [BO_4]. Dielectric constants of the samples might be an indication of the distortion in the coordinated boron atoms. The obtained experimental data indicated the internal structure of glass network and the change of the structure of the samples from three [BO_3] to four coordinated boron atoms [BO_4].

Keywords: borate glasses; Fourier transform infrared (FTIR) spectra; microhardness; thermal expansion; AC electrical properties

1 Introduction

Since the past several years, borate glasses have attracted much attention because of their electrochemical and optical applications, namely as solid-state batteries, optical wave guides and luminescent materials. Several previous works on borate glasses were devoted to study the structure, magnetic and electrical properties [1,2]. The glass materials, which consist of heavy metal oxides, such as lead, are more promising for photonics and optoelectronics. Depending on a kind of bond: ionic or covalent between lead and oxide, PbO plays the role as a modifier or a glass former. It is a function of PbO/B_2O_3 ratio in the glass. In order to stabilize glass network, many elements have been added to the base matrix. It has been very well known that iron [3], vanadyl [4], BaO [5], titanium dioxide [6] and copper [7] additions affect structure and glass properties in PbO–B_2O_3 system.

Lead borate glasses are good host matrix for rare-earth and transition-metal oxide. These glasses carry a great importance due to their promising

* Corresponding author.
E-mail: mmmsgomaa@yahoo.com

applications in the fields of laser technology, radiation shielding materials, luminescence materials, photonics and optoelectronic devices [8–10].

Lead borate oxide glasses are highly transparent in the visible and near-infrared regions and exhibit very good glass formation over a large compositional region [11]. Moreover, $PbO–B_2O_3$ glasses have desirable characteristics against irradiation, since the naturally occurring stable boron isotope is a good absorber of thermal neutrons [12] and lead is known as a shielding material of γ-rays [13]. It is now well known that lead oxide (PbO) is unique in its influence on the glass structure and is widely used in glasses, because it enhances the resistance against devitrification, improves the chemical durability and lowers the melting temperature [14]. It can act as either a glass network former or a modifier, depending on its concentration in the glasses [15].

Due to their potential applications in various domains of modern technology, glasses containing transition-metal oxides have been the subject of intensive investigations [16], for example, the glasses containing Fe_2O_3.

The co-existence of iron ions in more than one valence state, i.e., Fe^{2+} and Fe^{3+}, is a general condition for semiconducting behavior of borate glasses with these ions [17]. Consequently, glasses containing Fe_2O_3 are used in electrochemical, electronic, electro-optic and memory switching devices [18]. The addition of iron to borate glasses makes it electrically semiconducting and super paramagnetic [19].

The content of iron in diverse environments with different valence states that exist in the glass depends on the quantitative properties of modifiers and glass formers, size of the ions in the glass structure, their field strength, mobility of the modifier cation, etc. Hence, the correlation between the state and the position of the iron ion in the glass network and its physical properties is expected to be highly interesting [20].

The present work explores the dominant role of Fe_2O_3 on structural, physical and electrical properties in $Na_2O–PbO–B_2O_3$ glass system. Fourier transform infrared (FTIR) spectroscopy has been used to study the structure features and their effects on the density, molar volume, microhradness, thermal expansion and electrical properties. Therefore, the aim of this paper is to investigate the effect of increasing Fe_2O_3 at the expense of Na_2O on the structural, physical and electrical properties of sodium lead borate glasses.

2 Experimental

2.1 Preparation of glass

Analytically pure grade chemicals were used to prepare the following glass samples according to the molecular formula $x$$Fe_2O_3$–(25–$x$)$Na_2O$–25PbO–$50B_2O_3$ (in molar percentage) where x = 0, 5, 10 and 15. Fe_2O_3, Na_2CO_3, Pb_3O_4 and H_3BO_3 were mixed thoroughly. Each batch of formulas was weighed 50 g and melted in porcelain crucible placed in an electric furnace at temperatures ranging from 1000 ℃ to 1100 ℃ depending on the glass composition. Melting was continued under normal atmospheric condition for 2 h after the last addition of the batch constituents. The melts were swirled for every 30 min to ensure homogeneity and cast in rectangular forms, and all the samples were immediately transferred to annealing furnace at 400–450 ℃. The furnace was switched off and left to cool to room temperature.

2.2 Density and molar volume measurements

Density ρ of all glass samples was calculated by employing the Archimedes principle using xylene and applying the relationship:

$$\rho = \rho_b[W_a/(W_a - W_b)] \quad (1)$$

where W_a is the weight in air; W_b is the weight in xylene; and ρ_b is the density of xylene (ρ_b = 0.863 g/cm^3). The density data were used to calculate the molar volume V_M given by $V_M = M_T/\rho$, where M_T is the molecular weight of glass (in mol%); ρ is the density of glass [21].

The FTIR absorption spectra were recorded with JASCO FT/IR-300E spectrometer at room temperature in the range of 400–4000 cm^{-1} with a resolution of 4 cm^{-1} using the KBr pellet technique. In order to obtain good quality spectra, the samples were crushed in an agate mortar and the powders were pressed, and then the IR spectra were immediately measured.

Polished glass samples with dimension of 5 mm × 5 mm × 10 mm were used for linear thermal expansion measurements at a heating rate of 5 ℃/min by Linseis Thyristor-Stellglied 35V160V.23A analyzer. From these measurements, the thermal expansion coefficient α at 300 ℃ and both glass transition temperature T_g and dilatometric softening temperature T_s were determined.

The microhardness of the investigated samples was

measured by using Vicker's microhardness indenter (SHIMADZU, HMV-2 Series, Japan). The eye piece on the microscope of the apparatus allowed measurements with an estimated accuracy of ±0.5 mm for the indentation diagonals. The specimens were cut using a low speed diamond saw, dry ground using 1200 grit SiC paper, and polished carefully using 6 mm, 3 mm and 1 mm diamond pastes to obtain smooth and flat parallel surfaces of glass samples before indentation. At least, six indentation readings were made and measured for each sample. Testing was made using a load of 100 g; loading time was fixed for all glass samples (15 s). The measurements were carried out under normal atmospheric conditions. The Vicker's microhardness value H_V (kg/mm^2) was calculated using the following equation:

$$H_V = A(p/d^2) \quad (2)$$

where A is a constant value equal to 1854.5 (taking into account the geometry of squared based diamond indenter); p is the applied load (g); and d is the average diagonal length (mm).

2.3 Electrical measurements

Data were collected in the frequency range from 100 Hz up to 1 MHz using a Hioki 3522-50 LCR Hitester impedance analyzer contacted with one of the two electrodes shown in Fig. 1, which was a four electrode measurement. The measured parameters were the series and parallel capacitances and the series and parallel resistances at different frequencies (see Refs. [22–24] for more details).

In Fig. 1, A and B are the current electrodes, and M and N are the potential electrodes. They represent thin copper discs. The current and potential electrodes were immersed in the agar–agar/copper sulphate gel compartment [23]. Samples were connected to non-polarizable electrodes (Cu/$CuSO_4$) [23]. The oscillation amplitude was set at 1 V (small signal).

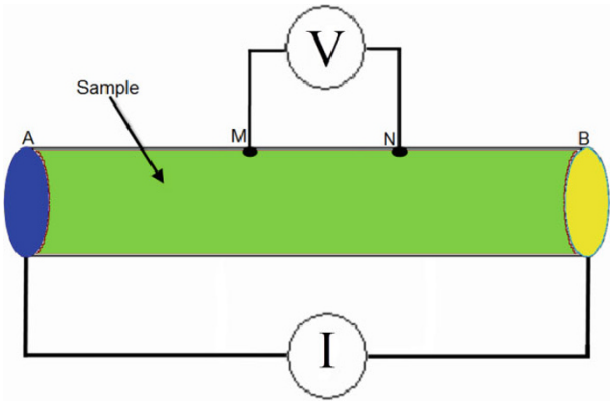

Fig. 1 A schematic representation of the sample holder.

Electrical properties of a material can be expressed in either series or parallel configuration [25]. The measured parameters were the parallel capacitance and conductance (C_p and G_p) and the series impedance Z at different frequencies (see Refs. [22–24] for more details). Measurements were done at room temperature at atmospheric relative humidity of ~50% in an isolated chamber (desiccator).

3 Results

3.1 Density and molar volume

The composition dependence of the density ρ of the present glass samples is shown in Fig. 2. It may be observed that density increases gradually with the increase of iron oxide content in the glass compositions. The relationship between density and composition of an oxide glass system can be expressed in terms of an apparent volume V_M occupied by 1 g atom of oxygen. The molar volume V_M of all the prepared glasses, is defined as the mean molecular weight M_T of its constituents divided by its experimental density, as given by the equation $V_M = M_T/\rho$. These values are also included in Table 1.

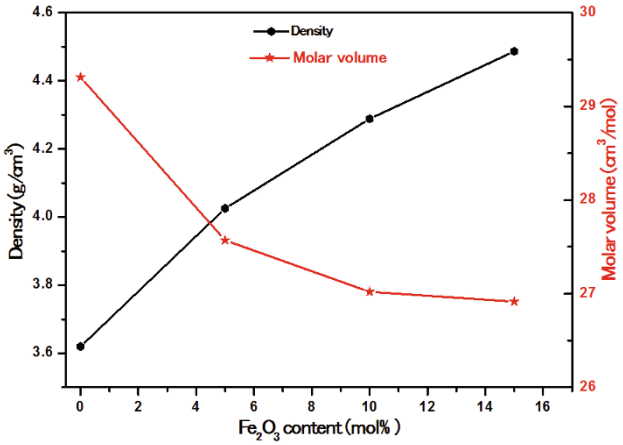

Fig. 2 Composition dependence of density and molar volume for the studied glasses.

Table 1 Chemical composition, density, molar volume, average boron–boron separation and microhardness of the investigated glasses

Glass No.	Glass composition (mol%)				Density (g/cm^3)	Molar volume (cm^3/mol)	$\langle d_{B-B} \rangle$ nm	Microhardness (kg/mm^2)
	Fe_2O_3	Na_2O	PbO	B_2O_3				
G_1	0	25	25	50	3.6200	29.3106	0.3651	374
G_2	5	20	25	50	4.0257	27.5703	0.3578	380
G_3	10	15	25	50	4.2884	27.0207	0.3553	429
G_4	15	10	25	50	4.4865	26.9166	0.3549	528

3.2 Infrared transmission spectra

Figure 3 illustrates the infrared spectra of the present glass systems. All the glass compositions show bands at 460 cm^{-1}, 575 cm^{-1}, 664 cm^{-1}, 711 cm^{-1}, 987 cm^{-1}, 1225 cm^{-1}, 1349 cm^{-1}, 1631 cm^{-1} and 3420 cm^{-1}.

3.3 Thermal expansion properties

The thermal expansion coefficient α, glass transition temperature T_g and dilatometric softening temperature T_s were determined in glasses containing different amounts of Fe_2O_3 at the expense of Na_2O and are summarized in Table 2 and Fig. 4.

The present results reveal that the increase in the amount of Fe_2O_3 at the expense of Na_2O leads to the decrease of the thermal expansion coefficient value and the increase of both T_g and T_s values (Table 2).

3.4 Microhardness

The present results indicate that the addition of Fe_2O_3 at the expense of Na_2O leads to the increase of microhardness value of the investigated glasses (Table 1).

3.5 Electrical measurements

The conductivity decreases with the increase of Fe_2O_3 at the expense of Na_2O replacement (at the same frequency). Figure 5 shows the variation of conductivity with frequency for different samples containing various proportions of Fe_2O_3 replacements. Slope for all samples is related to the increase of frequency. Figure 6 shows the variation of dielectric constant with frequency for different samples containing various proportions of Fe_2O_3 replacements. The increase of Fe_2O_3 replacements results in the increasing values of dielectric constants. Figure 7 shows the impedance plane with frequency for different samples containing various proportions of Fe_2O_3 at the expense of Na_2O. The equivalent circuit shown in Fig. 8 is assumed to represent the sample general structure.

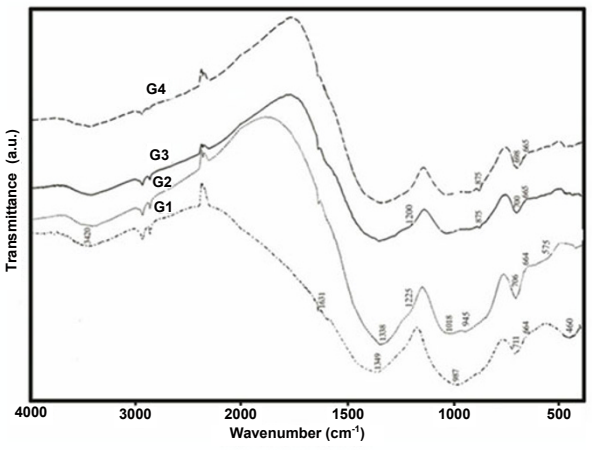

Fig. 3 Infrared transmission spectra of Fe_2O_3–Na_2O–PbO–B_2O_3 glasses.

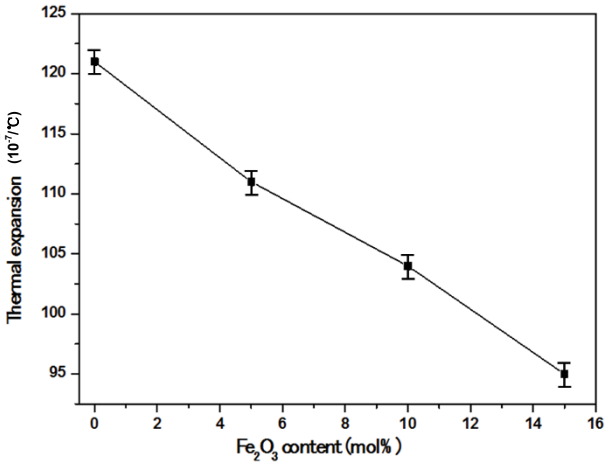

Fig. 4 Variation of thermal expansion coefficient of the glasses as a function of Fe_2O_3 content.

Table 2 Glass transition temperature, dilatometric softening temperature, thermal expansion coefficient, average coordination number and number of bonds per unit volume of the glass samples

Glass No.	T_g (℃)	T_s (℃)	α at 25–300 ℃ (10^{-7}℃$^{-1}$)	Average coordination number (m)	Number of bonds per unit volume n_b (10^{29}m^{-3})
G_1	352	374	121	3.25	0.6677
G_2	365	386	111	3.50	0.7645
G_3	375	395	104	3.75	0.8357
G_4	400	418	95	4.00	0.8949

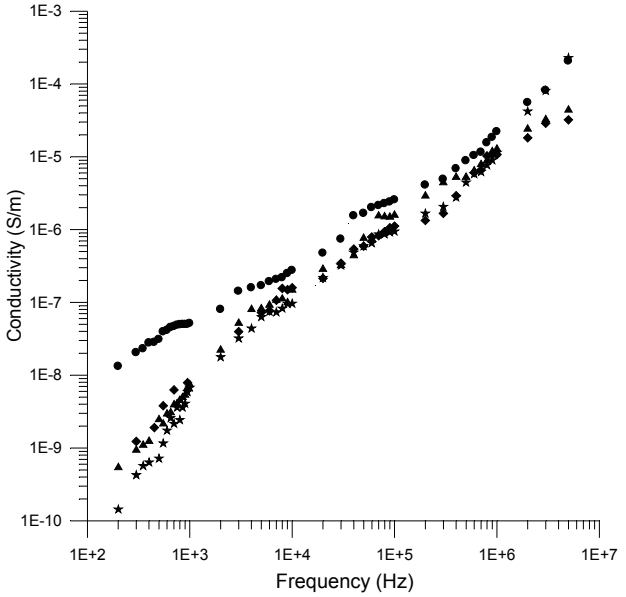

Fig. 5 Conductivity variation with frequency for samples G_1 (◆),G_2 (●), G_3 (▲) and G_4 (★).

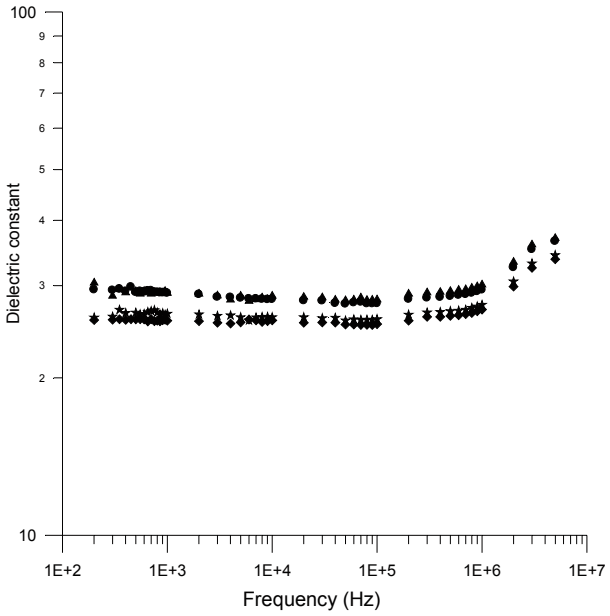

Fig. 6 Dielectric constant variation with frequency for samples G_1 (◆),G_2 (●), G_3 (▲) and G_4 (★).

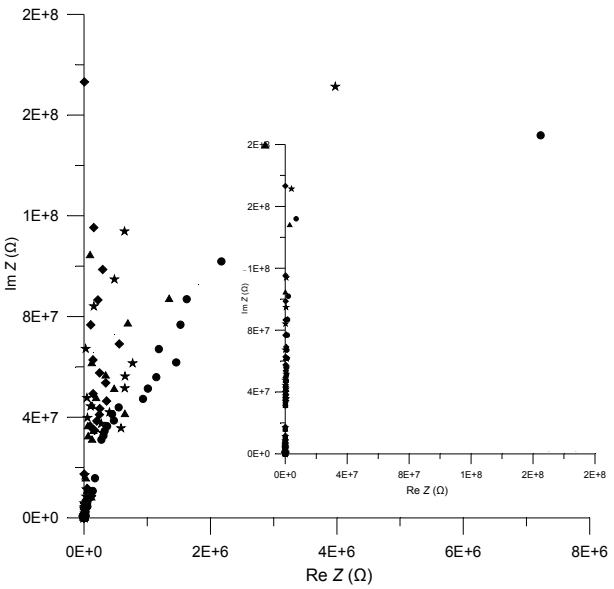

Fig. 7 Imaginary impedance variation with real impedance for samples G_1 (◆),G_2 (●), G_3 (▲) and G_4 (★).

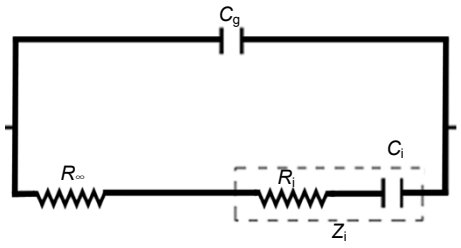

Fig. 8 Equivalent circuit that represents the sample (C_g and R_∞ are the capacitance and resistance of the sample at high frequency, respectively; C_i is the interfacial capacitance and R_i is the interfacial resistance).

4 Discussion

It is well known that pure B_2O_3 glass is composed essentially of [BO_3] triangles forming three-membered (boroxol) rings. By adding the modifier oxide to B_2O_3

glass, some [BO_3] triangles change to [BO_4] tetrahedra, breaking bridging oxygen bonds to form non-bridging oxygen (NBO) and residing in interstitial sites of the tetrahedral network in the vicinity of the negatively charged NBOs [26].

It is noted that borate glasses cannot be viewed as a simple network constructed only from [BO_3] triangles and/or [BO_4] tetrahedra [27]. Studies, where different experimental techniques were applied, have demonstrated that multi and complex borate glasses consist of relatively large structural units, such as boroxol, pentaborate, triborate, diborate and metaborate groups with bridging or non-bridging oxygen ion forms [1].

4. 1 Density and molar volume

As shown in Fig. 2, the density of glasses increases progressively with the decrease in molar volume due to addition of Fe_2O_3. The increase in density might be related to the replacement of Na_2O having lighter molecular mass with Fe_2O_3 having high molecular mass. The measured values of density and molar volume have been presented in Table 1. It shows how the compaction of glass network and higher molecular weight of Fe_2O_3 help to increase the density of glass samples. Another reason for increase in density may be the formation of more [BO_4] groups. The presence of iron oxide modifies the structural network by providing more oxygen, making conversion of [BO_3] to [BO_4] units [28]. Hence, it leads to an increase in density of the glass samples. The molar volume also plays good role. A decrease in molar volume leads to decrease in bond length which is responsible for compaction of glass network [29].

In order to confirm the compaction of glasses due to the presence of iron oxide, the average boron–boron separation ‹$d_{B–B}$› has been calculated [30]. The volume V_M^B corresponds to the volume that contains one mole of boron within the given structure and it can be stated as

$$V_M^B = \frac{V_M}{2(1 - X_B)} \tag{3}$$

where V_M is the molar volume; X_B is the molar fraction of B_2O_3.

$$\langle d_{B\text{-}B} \rangle = \left(\frac{V_M^B}{N_A} \right)^{\frac{1}{3}} \tag{4}$$

where N_A is the Avogadro number.

The calculated values of the average boron–boron separation are shown in Table 1. It can be observed that when the Fe_2O_3 content increases, the average boron–boron separation decreases. Consequently, the addition of Fe_2O_3 leads to compaction of glass network which confirms the results in terms of density and molar volume [29].

4. 2 Infrared transmission spectra

IR spectroscopy ranks among the rather sensitive methods of structure investigation of glasses. The application of this method makes it possible to obtain information on the structural role of oxides entering into the composition of glass, the change in the polymerization of the anion carcass with a change in the glass composition, and the coordination state of ions [31].

Figure 3 shows infrared transmission spectra in the 400–4000 cm^{-1} region for sodium lead borate glasses. Infrared bands are mainly related to vibrations of [BO_3] and [BO_4] groups. The transmission band in the range of 400–650 cm^{-1} is assigned to B–O–B and Pb–O–B bending vibrations as well as borate ring deformation [32].

The infrared spectrum of glass sample G_1 free from iron is shown in Fig. 3. The spectra of these glasses have exhibited FeO_6 octahedral band due to ν_1 vibration at 575 cm^{-1}, which is present in our spectra starting with $x = 5$ [33,34]. Iron ions are glass modifier and enter the glass network by breaking up the B–O–B bonds, and the Fe^{3+} and Fe^{2+} ions occupy interstitial positions and introduce coordination defect with non-bridging oxygen ions. In this case, Fe^{3+} and Fe^{2+} ions are octahedrally coordinated [35].

All glasses show a peak at 664 cm^{-1}. This is attributed to the bending vibration of B–O–B linkage in the borate network, which is previously reported by many authors [36]. It may also due to the presence of Pb–O vibration of lead oxide [37]. It is also assumed that the band observed at 664–711 cm^{-1} is due to the B–O–B bending vibrations of [BO_3] triangles [38].

In sample G_1, the band at around 1349 cm^{-1} has been assigned to the stretching of trigonal [BO_3] units in meta, ortho and pyro-borate groups [37,39]. The position of this band is shifting towards the lower wavenumber at higher content of iron oxide in glass samples G_2 to G_4. The band centered at 987 cm^{-1} in glass sample G_1 is assigned to B–O stretching vibrations of tetrahedral [BO_4] units in different borate

groups [40]. With the initial addition of Fe_2O_3 (5 mol%) into the glass network, intensity of this band decreases in glass sample G_2. At the same time, the intensity of the band due to $[BO_3]$ structural units has been observed to increase at the expense of the band due to $[BO_4]$ units. This observation suggests a gradual increase in the content of divalent iron ions in the glass network that act as modifiers [20].

For further addition of Fe_2O_3 (10 mol% and 15 mol%) to glass samples, intensity of this band decreases (bands due to $[BO_3]$ units). At the same time, it has been observed that intensity of the band due to the BO_4 structural units increases at higher content of iron oxide. The absorption band arises in the region of 850–1100 cm^{-1} indicating B–O bond stretching of the tetrahedra $[BO_4]$ units [38,41].

The predominant absorption band around the 850–987 cm^{-1} is related to the symmetrical stretching vibration of $[BO_4]$ units [42,43]. The transmission band at 1225 cm^{-1} is specific to the B–O stretching vibrations of $[BO_3]$ triangular units with non-bridging oxygen atoms [44,45]. This band shifts toward smaller wavenumber (glass samples G_3 and G_4) because of the increasing coordination number around B atoms [46].

The observed transmission bands from 1400 cm^{-1} to 1600 cm^{-1} can be ascribed to the B–O stretching vibrations in $[BO_3]$ units from metaborate, pyroborate, orthoborates and groups containing a large number of NBOs [42,45] which are disappeared with increasing iron oxide content.

So the presence of iron oxide modifies the structural network by providing more oxygen, which results in conversion of $[BO_3]$ to $[BO_4]$ units [29]. As a result, introduction of iron increases the cross linking of the glass matrix due to the increasing the number of tetrahedral $[BO_4]$ groups in the glass system. The infrared transmission peak observed in the region of 2500–4000 cm^{-1} is attributed to water groups OH stretching vibrations [29].

The $[BO_3]$ units in the iron sodium lead borate glasses prefer a coordination change to $[BO_4]$ rather than producing NBOs. The four-fold boron atoms are favored in the investigated system as compared with the three-fold ones [47].

4.3 Average coordination number

The average coordination number is an important parameter to confirm the bridging or non-bridging oxygen bond. The average coordination number (m) is calculated with the help of the equation [29]:

$$m = \sum n_{ci} X_i \tag{5}$$

where n_{ci} is the coordination of cation. The coordination numbers of boron, lead, sodium and iron cations are 4, 4, 1 and 6, respectively. The observed value of average coordination number of glass samples increases with the incorporation of iron oxide (Table 2). These results confirm that the Fe_2O_3 introduction in glass matrix progressively increases the number of bridging oxygen which causes an increase of $[BO_4]$ groups in glass network. As a result, the introduction of iron increases the cross linking of the glass matrix due to the increasing number of tetrahedral $[BO_4]$ groups in the glass system.

4.4 Bond density

The addition of Fe_2O_3 affects the number of bonds per unit volume and it can be calculated by the relation [29]:

$$n_b = \frac{N_A}{V_M} \sum n_{ci} X_i \tag{6}$$

where N_A is the Avogadro number; n_{ci} is the coordination number of cation; and X_i is molar fraction of different oxides. The obtained result (Table 2) shows the value of number of bonds per unit volume increases with the increase in iron content. It reveals clearly that iron ion plays the role of a modifier in the present glass system by creating more B–O bond vibrations of $[BO_4]$ groups. All these results are in good agreement with the FTIR measurements.

4.5 Thermal expansion, softening temperature and glass transition temperature

Thermal expansion is a very important thermal property of glass. The thermal expansion of glass is controlled by the asymmetry of the amplitude of thermal vibrations in the glass. It decreases as the rigidity of the glass network increases [48]. An increase of the number of non-bridging bonds weakens the structure, which in turn increases the thermal expansion coefficient, whereas the change in coordination number of the network former cation may cause either its increase or decrease depending on the effect on glass structure [49]. The cation B^{3+} is capable of changing its coordination number, which in turn

influences the structure and properties of the investigated glasses [31]. The anomaly tendency of the thermal expansion correlates with the ratio of $[BO_4]$ to $[BO_3]$ structural unit formation [48,49].

In this study, the thermal expansion coefficient gradually decreases by increasing Fe_2O_3 at the expense of Na_2O (Fig. 4). While, both T_g and T_s values are increased. This could be explained on the basis that the Fe_2O_3 introduction in glass matrix progressively increases the number of bridging oxygen which causes an increase of $[BO_4]$ groups in glass network, leading to a tightening of the network as indicated from FTIR spectra, resulting in the decrease of thermal expansion coefficient and the increase of both T_g and T_s values.

4.6 Electrical properties of the studied samples

Electrical measurements of the studied glasses were conducted in the frequency range from 100 Hz up to 1 MHz at room temperature (~20 ℃). Generally, the values of conductivity and dielectric constant of the samples are very close to each other. That means that the structure of the samples does not change with the adding of Fe_2O_3 at the expense of Na_2O in sodium lead borate glasses (from the electrical point of view) [50]. PbO content is constant through all the batch compositions, so we did not study its effect on the structure.

The conductivity decreases with the increase of Fe_2O_3 at the expense of Na_2O replacements (at the same frequency). Figure 5 shows the variation of conductivity with frequency for different samples containing various proportions of Fe_2O_3 replacements. It can be noticed that the change of composition affects the electrical properties due to the increase of Fe_2O_3 replacements of samples. The increase of Fe_2O_3 replacements results in the decrease in the conductivity. The decrease of conductivity may be due to the remarkable increase in the cross linking of the glass structures which increases its strength, due to converting three coordinated boron atoms $[BO_3]$ to four coordinated boron atoms $[BO_4]$ from G_1 to G_4.

Figure 5 shows a slope for all samples which is related to the increase of frequency. Figure 6 shows the variation of dielectric constant with frequency for samples containing various proportions of Fe_2O_3 replacements. The increase of Fe_2O_3 replacements results in the increase of the values of dielectric constants.

That increase is found by the progressive substitution of Fe_2O_3 at the expense of Na_2O that results in the replacement of three coordinated boron atoms $[BO_3]$ to four coordinated boron atoms $[BO_4]$, i.e., capacity of capacitors will increase. Also, the increase in the dielectric constant may be due to the increase in its strength of the investigated glasses.

Figure 7 shows the impedance plane with frequency for samples containing various proportions of Fe_2O_3 at the expense of Na_2O. Such impedance plane curves may be used as an indicator of the change in the internal structure of samples (continuous and broken paths or links). It is clear that the curves of impedance plane do not change greatly with the increase of proportions of Fe_2O_3 contents (Fig. 7). As the continuous conducting paths or links decrease (by increasing of Fe_2O_3/Na_2O replacements), the values of the imaginary part slightly decrease and the values of the real part decrease [50].

The equivalent circuit shown in Fig. 8 is assumed to represent the sample general structure. The conducting ions are completely insulated (blocked) from each other. Here, C_g and R_∞ represent the capacitance and resistance of the sample at high frequencies, respectively, where no space charges accumulate. C_i is the interfacial capacitance (frequency independent) and R_i is the interfacial resistance. The resistance decreases as the frequency increases at frequencies lower than the radio frequency range, where space charges are accumulated at interfaces. It is supposed that there is no direct conducting path between the two electrodes.

5 Conclusions

The FTIR study confirms that with the incorporation of iron oxide, $[BO_3]$ groups get converted into $[BO_4]$ groups. Change in the structure of glasses is also confirmed from the shifting of the bands and change in intensity with the addition of Fe_2O_3. The density of the glass samples increases with the increase of the Fe_2O_3 content and that causes a corresponding decrease in the molar volume. It may be attributed to the compaction of glass structure and formation of tetrahedral $[BO_4]$ groups.

The electrical properties of the studied samples are investigated in the frequency range from 100 Hz up to

1 MHz, and the effect of change in composition (Fe_2O_3 at the expense of Na_2O contents) on the measured properties is investigated. The increase of Fe_2O_3 replacements generally decreases the conductivity and increases the dielectric constant of the studied glasses. The obtained electrical data indicate the internal structure of glass network and the change in the structure of samples from [BO_3] to [BO_4].

References

[1] Pisarski WA, Goryczka T, Wodecka-Duś B, *et al*. Structure and properties of rare earth-doped lead borate glasses. *Mat Sci Eng B* 2005, **122**: 94–99.

[2] Agarwal A, Seth VP, Gahlot PS, *et al*. Effect of Bi_2O_3 on EPR, optical transmission and DC conductivity of vanadyl doped alkali bismuth borate glasses. *J Phys Chem Solids* 2003, **64**: 2281–2288.

[3] Farouk H, Solimani AA, Aly SA, *et al*. Role of iron addition on structure and electrical and magnetic properties of lithium lead borate glasses. *Mat Sci Eng B* 1996, **38**: 217–221.

[4] Kumar RR, Bhatnagar AK, Rao JL. EPR of vanadyl ions in alkali lead borate glasses. *Mater Lett* 2002, **57**: 178–182.

[5] Lee SW, Shim KB, Auh KH. Effects of BaO on the glass formation of the PbO–B_2O_3–TiO_2–BaO system in relation to transition temperatures. *J Mater Sci* 2002, **37**: 2011–2016.

[6] Koudelka L, Mošner P, Zeyer M, *et al*. Lead borophosphate glasses doped with titanium dioxide. *J Non-Cryst Solids* 2003, **326–327**: 72–76.

[7] Metwalli E. Copper redox behavior, structure and properties of copper lead borate glasses. *J Non-Cryst Solids* 2003, **317**: 221–230.

[8] Pisarska J, Pisarski WA, Ryba-Romanowski W. Laser spectroscopy of Nd^{3+} and Dy^{3+} ions in lead borate glasses. *Opt Laser Technol* 2010, **42**: 805–809.

[9] Pisarska J. Luminescence behavior of Dy^{3+} ions in lead borate glasses. *Opt Mater* 2009, **31**: 1784–1786.

[10] Saddeek YB. Structural and acoustical studies of lead sodium borate glasses. *J Alloys Compd* 2009, **467**: 14–21.

[11] Ciceo-Lucacel R, Ardelean I. FT-IR and Raman study of silver lead borate-based glasses. *J Non-Cryst Solids* 2007, **353**: 2020–2024.

[12] Sears VF. Neutron scattering lengths and cross sections. *Neutron News* 1992, **3**: 26–37.

[13] Ushida H, Iwadate Y, Hattori T, *et al*. Network structure of B_2O_3–PbO and B_2O_3–PbO–$PbBr_2$ glasses analyzed by pulsed neutron diffraction and Raman spectroscopy. *J Alloys Compd* 2004, **377**: 167–173.

[14] Ganguli M, Rao KJ. Structural role of PbO in Li_2O–PbO–B_2O_3 glasses. *J Solid State Chem* 1999, **145**: 65–76.

[15] Rao KJ, Rao BG, Elliott SR. Glass formation in the system PbO–$PbCl_2$. *J Mater Sci* 1985, **20**: 1678–1682.

[16] Chakradhar RPS, Sivaramaiah G, Rao JL, *et al*. Fe^{3+} ions in alkali lead tetraborate glasses—an electron paramagnetic resonance and optical study. *Spectrochim Acta A* 2005, **62**: 51–57.

[17] Moustafa YM, El-Egili K, Doweidar H, *et al*. Structure and electric conduction of Fe_2O_3–P_2O_5 glasses. *Physica B* 2004, **353**: 82–91.

[18] Mansour E, Moustafa YM, El-Damrawi GM, *et al*. Memory switching of Fe_2O_3–BaO–V_2O_5 glasses. *Physica B* 2001, **305**: 242–249.

[19] Collins DW, Mulay LN. Precipitation and magnetic behavior of beta $NaFeO_2$ in glasses along the Na_2SiO_3–Fe_2O_3 join. *J Am Ceram Soc* 1971, **54**: 69–72.

[20] Veerabhadra Rao A, Laxmikanth C, Appa Rao B, *et al*. Dielectric relaxation and a.c. conduction phenomena of PbO–PbF_2–B_2O_3 glasses doped with FeO. *J Phys Chem Solids* 2006, **67**: 2263–2274.

[21] Chimalawonga P, Kaewkhao J, Kedkaew C, *et al*. Optical and electronic polarizability investigation of Nd^{3+}-doped soda-lime silicate glasses. *J Phys Chem Solids* 2010, **71**: 965–970.

[22] Gomaa MM. Saturation effect on electrical properties of hematitic sandstone in the audio frequency range using non-polarizing electrodes. *Geophys Prospect* 2009, **57**: 1091–1100.

[23] Gomaa MM, Alikaj P. Effect of electrode contact impedance on A.C. electrical properties of wet hematite sample. *Mar Geophys Res* 2009, **30**: 265–276.

[24] Gomaa MM. Chapter 1: Factors affecting electrical properties of some rocks. In *Horizons in Earth Science Research*, *Volume 6*. Veress B, Szigethy J, Eds. New York: Nova Science Publishers, Inc., 2012.

[25] Gomaa MM, Abo-Mosallam HA, Darwish H. Electrical and mechanical properties of alkali barium titanium alumino borosilicate glass-ceramics containing strontium or magnesium. *J Mater Sci: Mater El* 2009, **20**: 507–516.

[26] Stefan R, Culea E, Pascuta P. The effect of copper ions addition on structural and optical properties of zinc borate glasses. *J Non-Cryst Solids* 2012, **358**: 839–846.

[27] Uchino T, Yoko T. Ab initio molecular orbital calculations on the structure and the low-frequency vibrational modes in B_2O_3 and alkali borate glasses. Borate Glasses Crystals and Melts International Conference, Society of Glass Technology, Sheffield, 1997: 417–424.

[28] Pal Singh G, Singh DP. Spectroscopic study of ZnO doped CeO_2–PbO–B_2O_3 glasses. *Physica B* 2011, **406**: 3402–3405

[29] Singh DP, Singh GP. Conversion of covalent to ionic behavior of Fe_2O_3–CeO_2–PbO–B_2O_3 glasses for ionic and photonic application. *J Alloys Compd* 2013, **546**: 224–228.

[30] Singh GP, Kaur P, Kaur S, *et al*. Conversion of covalent to ionic character of V_2O_5–CeO_2–PbO–B_2O_3 glasses for solid state ionic devices. *Physica B* 2012, **407**: 4269–4273.

[31] Bobkova NM, Khot'ko SA. Structure of zinc-borate low-melting glasses derived from IR spectroscopy data. *J Appl Spectrosc* 2005, **72**: 853–857.

[32] El-Alaily NA, Mohamed RM. Effect of irradiation on some optical properties and density of lithium borate glass. *Mat Sci Eng B* 2003, **98**: 193–203.

[33] Sambasiva Rao K, Krishna Mohan N, Veeraiah N. Physical properties of $(Li_2O)_{0.40}(Fe_2O_3)_{0.05-x}(P_2O_5)_{0.55}$: $(Ag_2O)_x$ glasses. *Turk J Phys* 2007, **31**: 11–30.

[34] Fang X, Ray CS, Marasinghe GK, *et al*. Properties of mixed Na_2O and K_2O iron phosphate glasses. *J Non-Cryst Solids* 2000, **263–264**: 293–298.

[35] Kashif I, Rahman SA, Mostafa AG, *et al*. Structural analysis and physical properties of iron–molybdenum lithium-borate glasses. *J Alloys Compd* 2008, **450**: 352–358.

[36] Singh SP, Chakradhar RPS, Rao JL, *et al*. EPR, FTIR, optical absorption and photoluminescence studies of Fe_2O_3 and CeO_2 doped ZnO–Bi_2O_3–B_2O_3 glasses. *J Alloys Compd* 2010, **493**: 256–262.

[37] Rada M, Rada S, Pascuta P, *et al*. Structural properties of molybdenum-lead-borate glasses. *Spectrochim Acta A* 2010, **77**: 832–837.

[38] Rajyasree Ch, Rao DK. Spectroscopic investigations on alkali earth bismuth borate glasses doped with CuO. *J Non-Cryst Solids* 2010, **357**: 836–841.

[39] Gandhi Y, Sudhakar KSV, Nagarjuna M, *et al*. Influence of WO_3 on some physical properties of MO–Sb_2O_3–B_2O_3 (M = Ca, Pb and Zn) glass system. *J Alloys Compd* 2009, **485**: 876–886.

[40] Gaafar MS, El-Aal NSA, Gerges OS, *et al*. Elastic properties and structural studies on some zinc-borate glasses derived from ultrasonic, FT-IR and X-ray techniques. *J Alloys Compd* 2009, **475**: 535–542.

[41] Sharma G, Singh K, Manupriya, *et al*. Effect of gamma irradiation on optical and physical properties of PbO–Bi_2O_3–B_2O_3 glasses. *Radiat Phys Chem* 2006, **75**: 959–966.

[42] Saritha D, Markandeya Y, Salagram M, *et al*. Effect of Bi_2O_3 on physical, optical and structural studies of ZnO–Bi_2O_3–B_2O_3 glasses. *J Non-Cryst Solids* 2008, **354**: 5573–5579.

[43] Gao G, Hu L, Fan H, *et al*. Effect of Bi_2O_3 on physical, optical and structural properties of boron silicon bismuthate glasses. *Opt Mater* 2009, **32**: 159–163.

[44] Simon V, Spinu M, Stefan R. Structure and dissolution investigation of calcium–bismuth–borate glasses and vitroceramics containing silver. *J Mater Sci*: *Mater M* 2007, **18**: 507–512.

[45] Karthikeyan B, Philip R, Mohan S. Optical and non-linear optical properties of Nd^{3+}-doped heavy metal borate glasses. *Opt Commun* 2005, **246**: 153–162.

[46] Fan H, Wang G, Hu L. Infrared, Raman and XPS spectroscopic studies of Bi_2O_3–B_2O_3–Ga_2O_3 glasses. *Solid State Sci* 2009, **11**: 2065–2070.

[47] Pascuta P, Pop L, Rada S, *et al*. The local structure of bismuth borate glasses doped with europium ions evidenced by FT-IR spectroscopy. *J Mater Sci*: *Mater El* 2008, **19**: 424–428.

[48] Gavriliu G. Thermal expansion and characteristic points of –Na_2O–SiO_2 glass with added oxides. *J Eur Ceram Soc* 2002, **22**: 1375–1379.

[49] Singh SP, Karmakar B. Synthesis and characterization of low softening point high Bi_2O_3 glasses in the K_2O–B_2O_3–Bi_2O_3 system. *Mater Charact* 2011, **62**: 626–634.

[50] Gomaa MM. Relation between electric properties and water saturation for hematitic sandstone with frequency. *Annals of Geophysics* 2008, **51**: 801–811.